Meteoritics & Planetary Science 1-17 (2025) doi: 10.1111/maps.70054

New knowledge about shock events that affected the L-chondrite parent body from two heavily shocked L6 meteorite finds

I. BAZIOTIS 1, L. FERRIÈRE 2,3, C. MA 1, J. HU 1, D. PALLES, and P. D. ASIMOW

¹Department of Natural Resources Management and Agricultural Engineering, Agricultural University of Athens, Athens, Greece

²Natural History Museum Vienna, Vienna, Austria ³Natural History Museum Abu Dhabi, Abu Dhabi, United Arab Emirates ⁴Division of Geological and Planetary Sciences, California Institute of Technology, Pasadena, California, USA ⁵Theoretical & Physical Chemistry Institute, National Hellenic Research Foundation, Athens, Greece

*Correspondence

I. Baziotis, Department of Natural Resources Management and Agricultural Engineering, Agricultural Univ. of Athens, Iera Odos 75, Athens 11855, Greece.

Email: ibaziotis@aua.gr

(Received 14 August 2025; revision accepted 13 September 2025)

Abstract—We report new results from a study of shock-related features in the L6 ordinary chondrites Northwest Africa (NWA) 4672 and NWA 12841. Our observations confirm the occurrence of eight high-pressure (HP) minerals in each meteorite, namely, ringwoodite, majorite, akimotoite, wadsleyite, albitic jadeite, lingunite, tuite, and xieite. Based on the calibration of phase stability fields and majorite chemical variations from static experiments, we estimate peak shock conditions of 18–23 GPa and 1800–2100°C. However, both meteorites also contain minerals thought to record lower pressures, 14-18 GPa for wadsleyite, and possibly ~11.5 GPa for albitic jadeite. These are interpreted to have formed by cooling during partial release from the peak shock state. Although the presence of discrete shock melt veins demands spatial heterogeneity in the temperature field, we interpret the record of HP mineralogy in terms of temporal rather than spatial variation in pressure-temperature conditions during the shock and release event. Specifically, we infer that the cooling of shock melt veins to their liquidus occurred near peak pressure, whereas decompression began before the melt veins reached their solidus. NWA 4672 and NWA 12841 also display dense networks of shock melt veins, metal-sulfide segregations, and dark shock zones, implying a high density of pre-existing weak zones and, thus, a high likelihood of fragmentation during atmospheric entry. A comparison with the Suizhou L6 chondrite, in which a total of 26 HP phases have been identified, suggests that differences in the identification and number of observed HP polymorphs mostly reflect differences in the completeness and spatial scale of analytical studies rather than a true difference in the intensity of shock processing. It remains quite likely that many shocked L chondrites host more HP phases than have been recognized so far. These new results indicate a need for further high-resolution studies of L chondrites to distinguish between observational bias and true variations in the range of shock states they experienced.

INTRODUCTION

Shocked meteorites record the collisional evolution of asteroids and provide natural specimens allowing the discovery and characterization of high-pressure (HP) and high-temperature (HT) minerals. These HP and HT phases, including both minerals and amorphous materials, record the final results of the evolution of their

host meteorite through a series of states generated by the passage of shock and release waves. The occurrence, composition, assemblage, and texture of such phases help us to understand processes including the collisional evolution of the asteroid belt through time, the kinetics of mineral transformation during shock, and (of most interest to the broader geoscience community) the deep mantle mineralogy of terrestrial planets.

Although terrestrial samples of deep mantle mineralogy have been recovered as inclusions in superdeep diamonds (coming from depths of 300-1000 km; Akaogi, 2022 and references therein), these samples are exceedingly rare and include only a few of the known HP polymorphs likely to occur in the mantle. Experiments can also lead to the synthesis of HP phases before their discovery in nature (e.g., Stishov, 1961). Nonetheless, it is the search for and analysis of shock-induced minerals in meteorites that have led to the great majority of HP mineral discoveries (e.g., Ma, 2018). Thus, mineralogy of the shocked meteorites, especially the mineral assemblages hosted within their shock melt veins, has led to numerous insights explaining the seismic and geochemical properties of the Earth's mantle despite the difference of many orders of magnitude in time scale between shock synthesis and mantle dynamics.

The HP and HT phases identified to date in ordinary chondrite meteorites include polymorphs of olivine (ringwoodite, wadsleyite, poirierite, ahrensite, asimowite), pyroxene (majorite, akimotoite, hemleyite, bridgmanite, hiroseite, albitic jadeite), feldspar (lingunite, maskelynite), silica (coesite, stishovite), phosphate (tuite), and chromite (xieite, chenmingite, wangdaodeite) (Bindi et al., 2017; Bindi et al., 2019; Bindi et al., 2020; Binns et al., 1969; Chen et al., 2008; Chen & El Goresy, 2000; Chen, Shu, Mao, et al., 2003; Chen, Shu, Xie, et al., 2003; Ghosh et al., 2021; Gillet et al., 2000; Ma et al., 2016; Ma et al., 2019; Ma et al., 2022; Mason et al., 1968; Miyahara et al., 2017; Price et al., 1983; Putnis & Price, 1979; Saikia et al., 2022; Sazonova et al., 2006; Sharp et al., 1997; Smith & Mason, 1970; Tomioka & Fujino, 1997; Tomioka & Fujino, 1999; Tomioka et al., 2000; Tomioka et al., 2020; Tomioka & Okuchi, 2017; Tschauner et al., 2009; Tschauner et al., 2014; Xie et al., 2020; Xie, Minitti, et al., 2002; Xie, Tomioka, et al., 2002). A range of meteorite classes and petrographic types host such phases, but it is clearly the L6 ordinary chondrites that yield the greatest abundance and variety of HP phases (e.g., Simopoulou et al., 2025; Xie et al., 2025). The simplest explanation for this observation may be that L6 ordinary chondrite precursors experienced higher pressure (P)-temperature (T) shock conditions than any other group of chondrites, at least within their shock melt veins. However, shocks beyond a certain P-T range are likely to become less suitable for preserving HP phases after recovery and annealing processes (Hu & Sharp, 2022), so it may be more appropriate to say that the L6 ordinary chondrite precursors experienced more optimal shock conditions (as opposed to higher shock conditions) than other meteorite groups. It is also important to note that the apparent dominance of highly shocked L chondrites may partly reflect sampling bias, as many of the L chondrites recovered on Earth are linked to the Ordovician break-up event (e.g., Korochantseva et al., 2007; Schmitz et al., 2016).

We report here on the discovery of numerous HP phases in two L6 ordinary chondrites, Northwest Africa (NWA) 4672 (find from 2006; S4) and NWA 12841 (find from 2010; S4). Numerous shock melt veins (MVs) with variable thickness up to a maximum of ~500 µm occur in all studied polished sections of both meteorites. The MVs contain HP phases with the stoichiometry of olivine, pyroxene, plagioclase, garnet, phosphate, and chromite. Each of the identified phases has already been found in other meteorites with shock stages ranging from S3 to S5 (based on the Stöffler et al., 2018 shock classification). Each HP phase in an assemblage may have grown at any time and place in an evolving system of heterogeneous P and T conditions, either within its thermodynamic stability field or by a metastable growth process. We consider together the set of coexisting HP and HT phases and the constraints on P-T-time path arising from the size and texture of their host shock melt veins to define shock records that build the overall library of shock sequences experienced by the L chondrites in general.

MATERIALS AND METHODS

Material

One polished thin section of NWA 4672 (NHMW-N5851) and one polished thin section of NWA 12841 (NMHW-O1154) were studied with a focus on their shock melt veins. In NWA 4672, a total of nine regions of interest (ROIs) were investigated; seven of the ROIs belong to one thick melt vein (MV) parallel to the fusion crust, while the other two ROIs belong to another thinner MV perpendicular to the fusion crust. In NWA 12841, we analyzed a total of 17 ROIs in the widest MV present in the investigated section and in two thinner MVs.

Analytical Methods

We used optical microscopy, scanning electron microscopy (SEM) with energy-dispersive X-ray (EDS) analysis and electron backscatter diffraction (EBSD), electron probe microanalysis (EPMA), and Raman spectroscopy (RS). We used transmitted and reflected light microscopy to characterize the texture (e.g., to search for

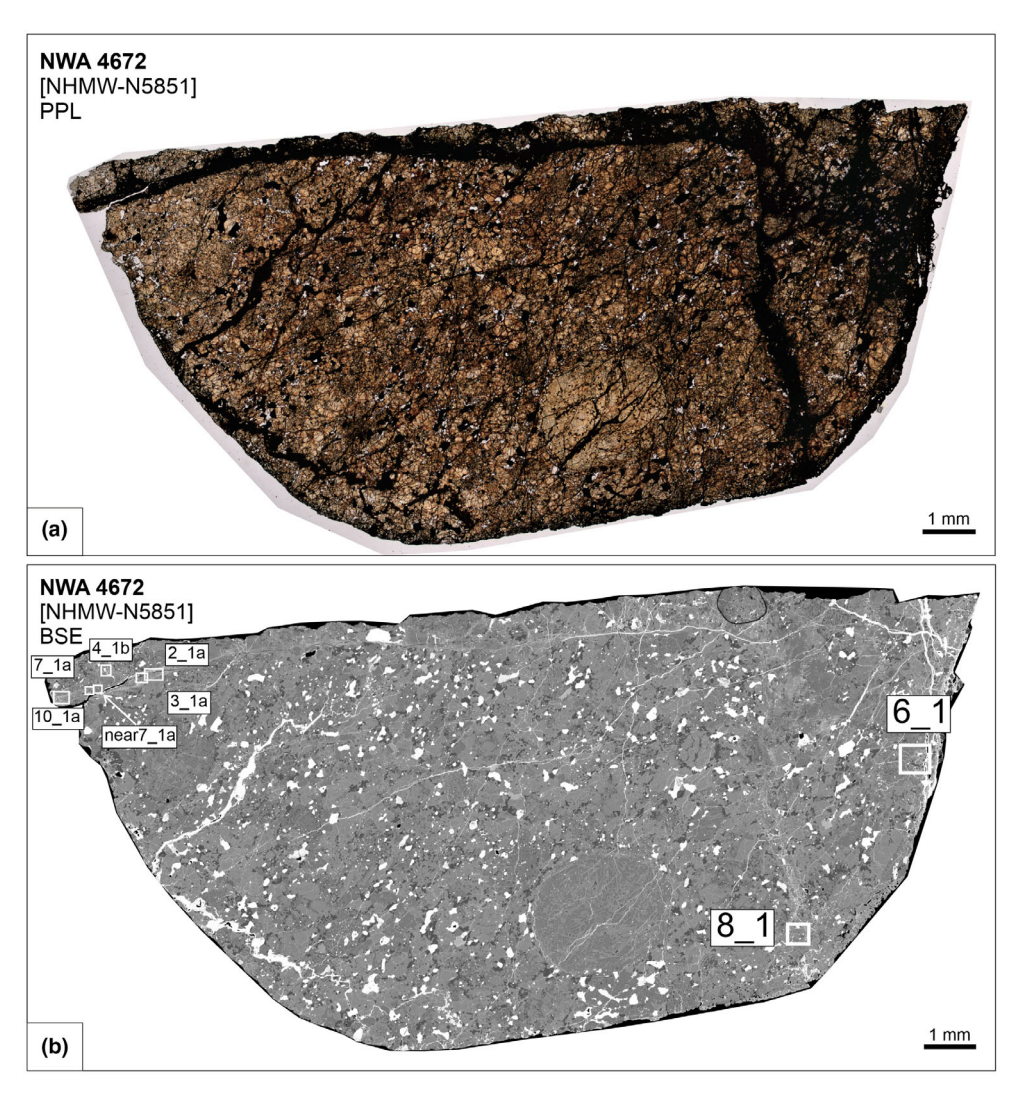


FIGURE 1. (a) Optical microscope (plane-polarized light) mosaic of the NWA 4672 section (NHMW-N5851) showing the MV network within the brecciated brownish groundmass. A large chondrule is visible at the bottom center of the image. (b) Backscattered electron mosaic of the NWA 4672 section showing the studied ROIs within the MVs.

relict chondrules) and coarse-grained mineralogy within or in contact with the MVs. We also applied conventional transmitted light microscopy criteria to evaluate the bulk rock deformation features in order to define the shock stage classification of the studied meteorites.

High-resolution thin section mosaics (Figures 1 and 2) were obtained using a uScopeGX-10 digital microscope scanner from Microscopes International at the Natural History Museum Vienna (NHMW; Austria). High-resolution backscattered electron (BSE) images were obtained using a JEOL JXA 8530F field-emission (FE) EPMA at the NHMW and a Zeiss 1550VP FE SEM at the California Institute of Technology (Caltech), United States, equipped with EBSD for the determination of crystal structure. Furthermore, mineral chemistry was determined using EPMA at the NHMW.

The probe spot size was $\sim 1~\mu m$ for olivine, pyroxene, chromite, and metal, whereas for plagioclase and phosphates, the beam was defocused ($\sim 3-5~\mu m$ diameter).

We also used a Renishaw InVia Confocal Raman microscope at the Mineral Spectroscopy Laboratory at Caltech (514.5 nm wavelength laser) and a Renishaw inVia Reflex at the Theoretical & Physical Chemistry Institute, National Hellenic Research Foundation (Athens, Greece), also using a 514.5 nm wavelength laser and a 2400 line mm $^{-1}$ diffraction grating. The laser was set to <2 mW power to avoid laser damage, knowing that some high-pressure (HP) phases and minerals are more or less sensitive. The laser spot size was typically $\sim 1-2~\mu m$. Each spectrum in the map was collected for 5 s with a 3000 line mm $^{-1}$ diffraction grating, spanning Raman shifts of 200–1100 cm $^{-1}$.

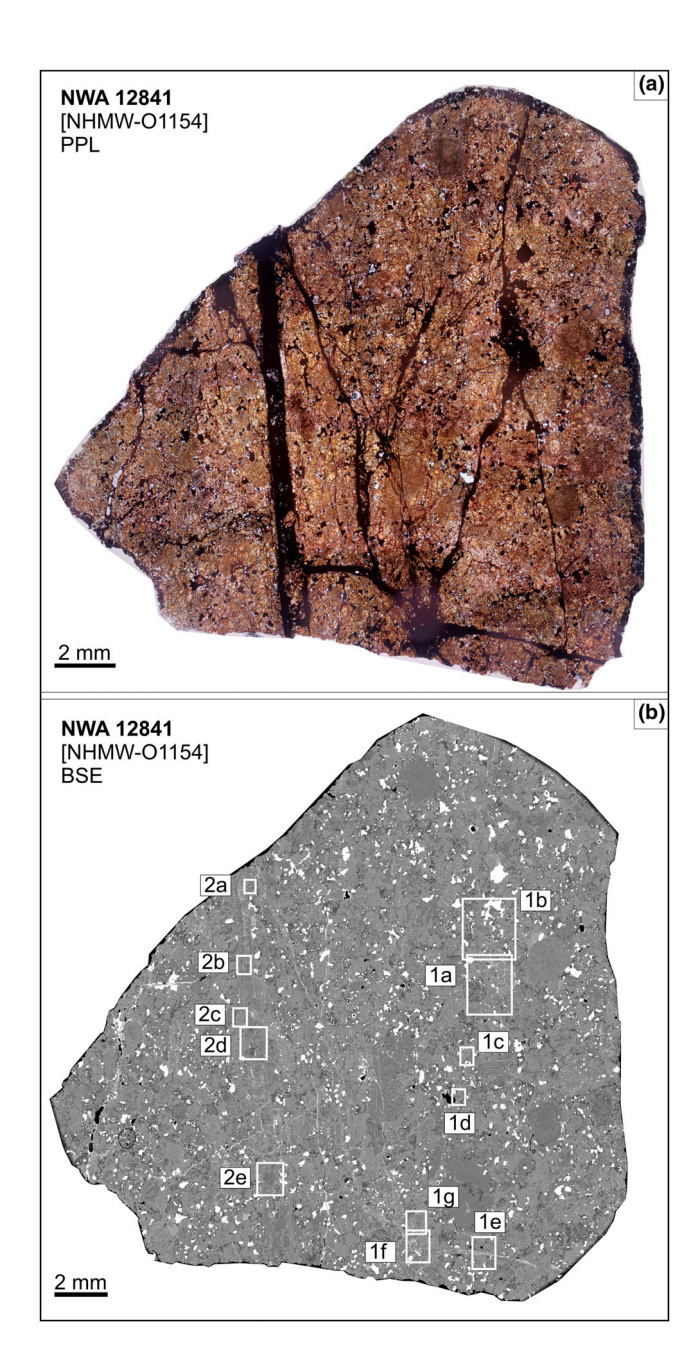


FIGURE 2. (a) Optical microscope (plane-polarized light) mosaic of the NWA 12841 section (NHMW-O1154) showing the thick MV, various thinner MVs, and two melt pockets. (b) Backscattered electron mosaic of the NWA 12841 section showing the studied ROIs within the MVs.

RESULTS

Petrography

NWA 4672

The groundmass of NWA 4672 is pale brown in color and consists mostly of recognizable chondrules and chondrule fragments ranging from 30 μ m to 3 mm in

diameter (Figure S1). The groundmass is heavily brecciated and shows several shock-related features. Olivine grains show weak to strong mosaicism and planar fractures. Plagioclase is converted to feldspathic glass. A dense network of pervasive veins, presumed to be the result of shock, cross-cut the groundmass chondrules and individual clasts (Figure 1). These features indicate that the meteorite was moderately and variably shocked from shock stage S3 to S5; however, the dominant shock stage (representing the largest area fraction of the investigated section) is S4 (Meteoritical Bulletin 113). The melt veins (MVs) have variable width, from ~40 to ~200 µm (Figure 1), are mostly crystalline (even at nm scale), and are made up of silicate clasts (mostly of olivine stoichiometry) plus silicate matrix, sulfides, and Fe-Ni metal grains (Figures 3a,b and 4). The MVs show characteristic gradation from glass-bearing rims through segregated metal-rich layers ~20 µm from the vein boundary to silicate-clast-rich cores. Most clasts within the veins show shape preferred orientation with their long axis parallel to the MV elongation.

NWA 12841

The groundmass of NWA 12841 is brownish in color with numerous indistinct chondrules, both complete and fragmentary (Figure 2). The more visible chondrules are barred olivine and porphyritic olivine-pyroxene types. The chondrules are embedded in a predominantly fine-grained, recrystallized groundmass containing merrillite and chlorapatite (up to ~150 µm in size) and minor opaque phases, including Fe-Ni metal, troilite, and fractured anhedral chromite grains. Thin oxide coatings surround Fe-Ni metal and troilite grains. There are numerous shock-related petrographic features. The olivine grains show weak to strong mosaicism, planar fractures, and planar deformation features, while plagioclase is converted to feldspathic glass. These features indicate that the meteorite was moderately and variably shocked from shock stage S3 to S5; however, the dominant shock stage (representing the largest area fraction of the investigated section) is S4 (Meteoritical Bulletin 108). A complex network of shock melt veins includes one thick MV (from 500 to 600 µm wide) and numerous thinner MVs with variable thickness (from ~40 to 100 μm) and random orientation. Several of the thin MVs emanate from two melt pockets (Figure 2). All the MVs are presumed to be the result of a single shock event because of the absence of cross-cutting relationships among them. The MVs mostly cut through olivine and orthopyroxene crystals and occasionally intersect groundmass metal grains. The MVs consist of glass, silicate clasts, sulfides, chromite, phosphate, and Fe-Ni metal grains. The zonation across the veins and the shape preferred orientation of the clasts are the same as described above for NWA 4672. In plane-polarized light,

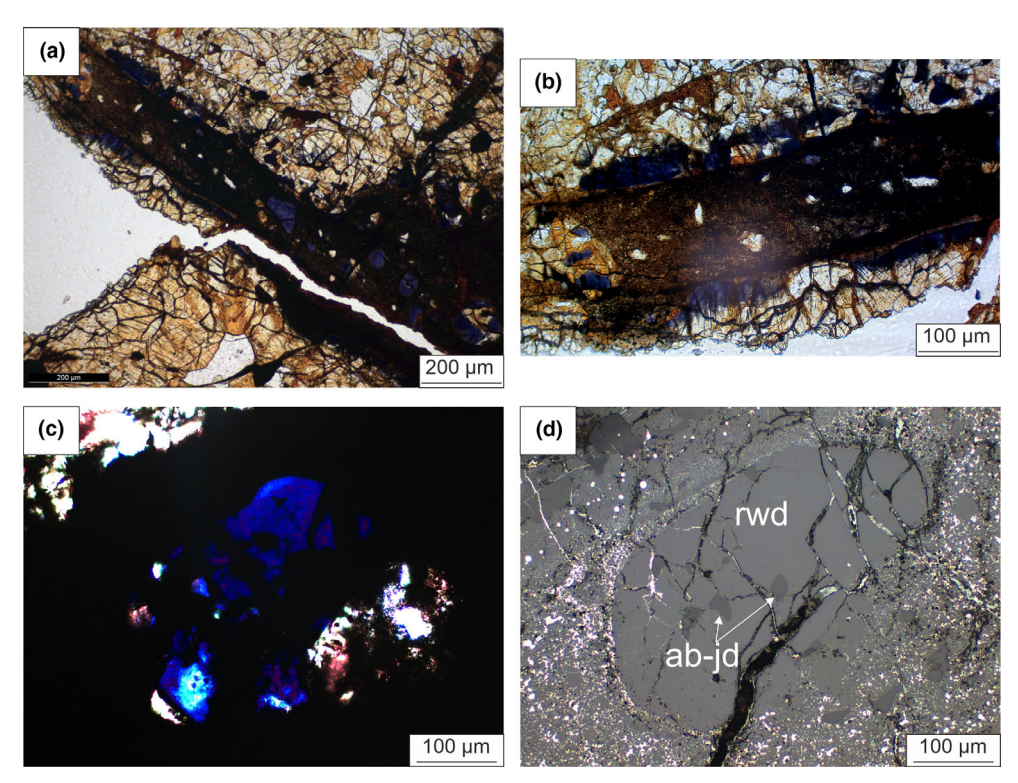


FIGURE 3. Optical microscope images of ringwoodite: (a) in NWA 4672 MV (in plane-polarized light); (b) in contact with the NWA 4672 groundmass (in plane-polarized light); (c) large clast within an MV from NWA 12841 (in cross-polarized light); (d) the same ringwoodite clast in NWA 12841 in reflected light.

large blue ringwoodite aggregate clasts (up to \sim 100 μ m in size) are clearly visible within the MVs (Figure 3c,d).

High-Pressure Polymorph Mineral Phases and their Chemistry

NWA 4672

We identified various mineral phases considered as definitive indicators of HP in the MVs in NWA 4672, including ringwoodite (rwd), wadsleyite (wds), majorite-pyrope_{ss} (maj), akimotoite (aki), lingunite (lin), albitic jadeite (ab-jd), xieite (xie), and tuite (tu).

Olivine Polymorphs

Ringwoodite crystallized from the MV is slightly more Mg-rich (Fo_{73.7–75.4}) compared to ringwoodite lamellae in the nearby transformed matrix olivine (Fo_{71.5–73.5}) (Figure 4a–c); the olivine from the chondritic portion of the meteorite is comparable to the ringwoodite from the MV (Fo_{74.5–75.5}). Wadsleyite occurs as sub- μ m crystals associated with majorite; they are too small for exact electron probe microanalysis (EPMA) (Figure 4a,b).

Pyroxene Polymorphs

Majoritic garnet yields EPMA composition of $Ca_{0.05-0.07}Mg_{3.15-3.19}Fe_{0.85-0.87}Al_{0.01}Si_{3.86-3.89}O_{12}$ (Figure 4a).

One analyzed grain displays a mixed Raman spectrum with both akimotoite and majorite peaks, but we could not identify a homogeneous akimotoite domain large enough for analysis by EPMA (Figure 4a). Albitic jadeite crystals (~40 µm long) form a rim that completely surrounds plagioclase glass (Figure 4b) and also occur in an irregular melt pocket along with lingunite (Figure 4d). Albitic has a formula jadeite $(Na_{0.59-0.67}Ca_{0.08}$ $K_{0.02-0.05}\square_{0.23-0.29}$) (Al_{0.79-0.84}Si_{0.15-0.18}Fe_{0.01-0.03})Si₂O₆ and Ca# (molar $100 \times \text{Ca/[Ca + Na]}$) varies from 10.4 to 11.4. The M2 vacancies and Si on M1 make this a typical example of albitic jadeite.

Plagioclase Polymorphs

Lingunite crystals (identified by Raman) occur along with albitic jadeite (Figure 4d); however, we could not acquire a pure lingunite analysis by EPMA.

Phosphate Polymorphs

Anhedral to subhedral $10-15 \mu m$ crystals of tuite have a merrillite composition, with MgO in the range of $\sim 3.5-3.7$ wt% (Figure 4e).

Chromite Polymorphs

Xieite occurs as small unoriented $1-2~\mu m$ crystals within chromite clasts; xieite is almost identical to

FIGURE 4. Backscattered electron images from NWA 4672 providing context for the acquired Raman spectra, given with corresponding numbers of spectra in Figure 6a. (a) Large clasts of shocked olivine (ol) and orthopyroxene (opx) are embedded in a groundmass of majorite and ringwoodite (ROI #6_1i as in Figure 1b). (b) An oval-shaped olivine clast transformed to ringwoodite and a feldspar clast transformed to lingunite and albitic jadeite lie in the central part of an MV, and majorite and wadsleyite occur toward the rim of the MV. Olivine in the adjacent groundmass contains ringwoodite lamellae (ROI #2_1a as in Figure 1b). (c) Groundmass olivine in contact with an MV contains rwd lamellae (ROI #7_1f as in Figure 1b). (d) An irregularly shaped clast of albitic jadeite and lingunite is surrounded by majoritic groundmass (ROI #6_11 as in Figure 1b). (e) Tuite and albitic jadeite are found in the central part of an MV (ROI #7_1a as in Figure 1b). (f) A large irregular chromite clast has domains of xieite (bright areas) (ROI #4_1b as in Figure 1b).

chromite host in composition, with Cr_2O_3 54.4–55.9 wt %, FeO 31.3–32.1 wt%, Al_2O_3 5.83–6.41 wt%, and TiO_2 2.40–2.95 wt% (Figure 4f).

NWA 12841

In MVs of NWA 12841, we identified all the same HP phases as observed in NWA 4672, but there are some notable differences in their compositional and textural details.

Olivine Polymorphs

The ringwoodite crystals within the melt veins (average Fo₇₀) are generally iron-rich compared to coexisting wadsleyite (average Fo₇₅) as well as the ringwoodite lamellae in matrix olivine in contact with the MV, Fo₇₂₋₇₅. This is the opposite of the compositional contrast in NWA 4672, where the MV ringwoodite is more Mg-rich than the matrix ringwoodite lamellae. Ringwoodite generally occurs in association with

9455100, 0, Downloaded from https://onlinelibrary.wiley.com/doi/10.1111/maps.70054 by Natl Hellenic Res Fndtn (NHRF), Wiley Online Library on [24/10/2025]. See the Terms

onlinelibrary, wiley, com/terms-and-conditions) on Wiley Online Library for rules of use; OA articles are governed by the applicable Creative Commons Licenso

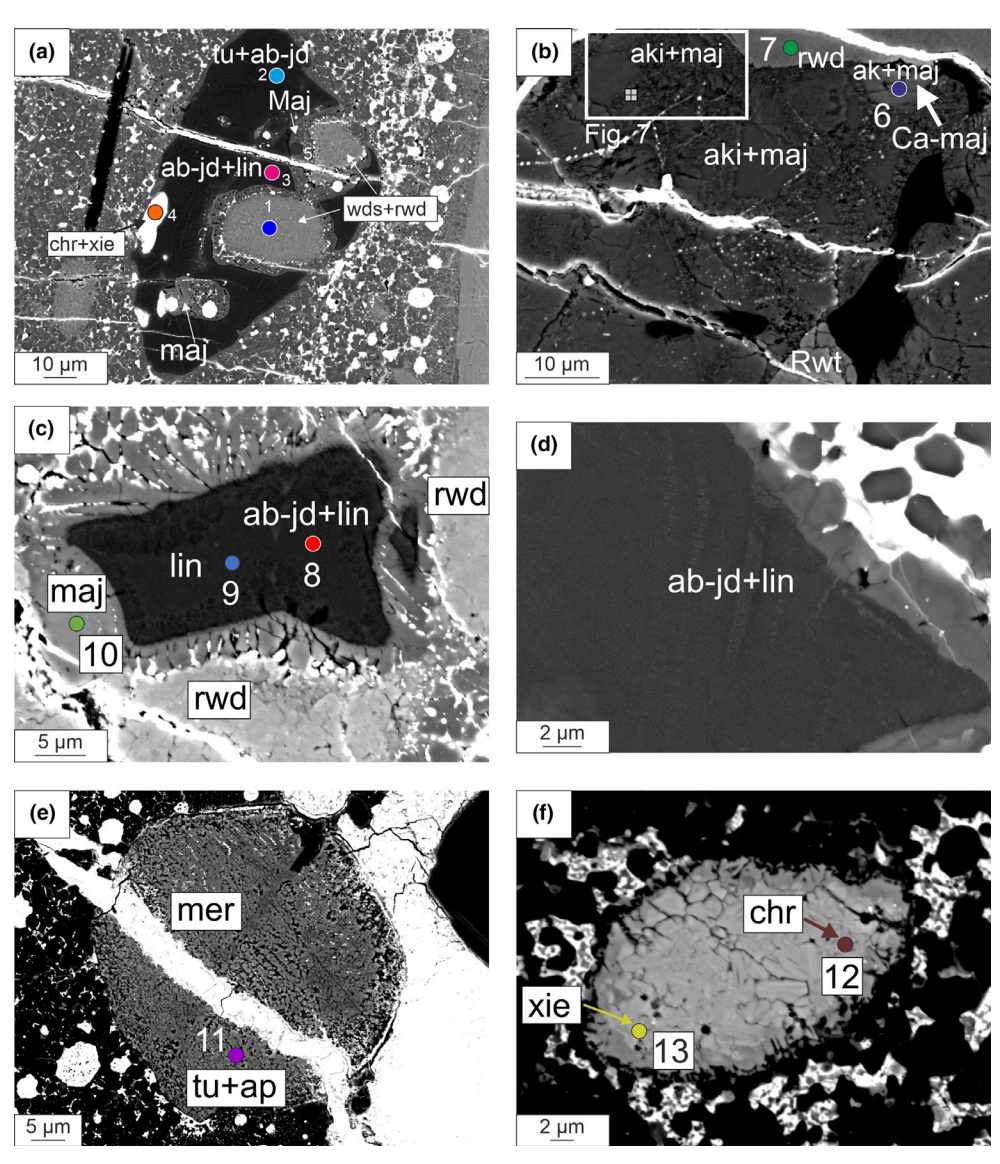


FIGURE 5. Backscattered electron images from NWA 12841; the numbered spots indicate acquisition spots for Raman spectra given in Figure 6b. (a) A composite clast is dominated by high-pressure polymorphs (ROI #1g as in Figure 2b). (b) A melt pocket is composed of majorite, akimotoite, Ca-rich majorite, and ringwoodite. The white rectangle was further investigated at high resolution in Figure 7, with an EBSD spot acquired at the small box with cross (ROI #2c as in Figure 2b). (c) A melt pocket solidified as lingunite and albitic jadeite surrounded by a halo of majorite, further rimmed by ringwoodite (ROI #1c as in Figure 2b). (d) Albitic jadeite and lingunite lamellae are intergrown within a small melt pocket (ROI #1b as in Figure 2b). (e) A rounded phosphate clast is composed of apatite, merrillite, and tuite (ROI #1c as in Figure 2b). (f) A fish-shaped chromite clast contains xieite domains (ROI #2a as in Figure 2b).

wadsleyite in rounded areas within oval-shaped segments of a large composite clast (Figure 5a) or as polycrystalline clasts (Figure 5b,c).

Pyroxene Polymorphs

The EPMA composition of garnet grains in the large MV indicates an average majoritic garnet composition of $Ca_{0.05}Mg_{3.14}Fe_{0.87}Al_{0.02}Si_{3.92}O_{12}$ (Figure 5a,b). Dark grains of albitic jadeite occur as sub- μ m lamellae or as

irregular crystallized areas ~10 μ m across within MVs (Figure 5a,c,d). EPMA of albitic jadeite gives the following range of empirical formulae: (Na_{0.60-0.66}Ca_{0.07-0.08} K_{0.04-0.07} $\square_{0.22-0.27}$) (Al_{0.81-0.86}Si_{0.15-0.17}Fe_{0.01-0.03})Si₂O₆ with Ca# from 10.2 to 11.3. One analyzed grain displays a Raman spectrum consistent with akimotoite (spectrum #6; see Raman Spectroscopy and EBSD section) but a Ca-rich pyroxene composition by EPMA, Ca_{0.83}Fe_{0.16}Mg_{0.98} Al_{0.02}Si_{1.98}O₆. We were not able to resolve whether this is a

novel high-Ca HP phase or a fine mixture of akimotoite and clinopyroxene.

Plagioclase Polymorphs

Lingunite occurs within domains of a melt pocket with or without albitic jadeite (Figure 5c). This phase proved too sensitive to electron beam damage to yield reliable EPMA. We observed alternating stripes (up to $1.5 \mu m$ wide) of lingunite and albitic jadeite radiating from the boundary of a small melt pocket of plagioclase composition (Figure 5d).

Phosphate Polymorphs

Minute single crystals (2–3 μ m; Figure 5e) of tuite are associated with apatite and merrillite within a rounded phosphate grain (~100 μ m in diameter). The EPMA composition of tuite shows MgO up to ~1.1 wt% and relatively high Cl content, either due to contamination from adjacent apatite or to inheritance from a partly chlorapatite precursor (Xie et al., 2013). Currently, based on the size of the inferred HP phase, it is impossible to conclude on the precursor of tuite in NWA 12841. It is important to note that the groundmass apatite has Cl up to ~5.3 wt%.

Chromite Polymorphs

Anhedral to subhedral chromite clasts up to $\sim 20~\mu m$ long demonstrate notable internal contrast in BSE images, with chromite appearing dark compared to brighter xieite domains (Figure 5f). However, the chemical compositions of both phases are identical and match that observed in NWA 4672. The BSE contrast presumably reflects the density difference between the polymorphs.

Raman Spectroscopy and EBSD

NWA 4672

We characterized eight HP minerals whose Raman spectra (RS) match the characteristic bands of reference spectra from the RRUFF database: rwd, wds, maj, aki, ab-jd (whose RS peaks match jadeite but whose composition does not), lng, xi, and tu (Figure 6a). Although the Raman spectra of ringwoodite (#1, #3, #4 in Figure 6a) from NWA 4672 are mixed with other phases, each shows the characteristic peaks at 795-799 and 842-844 cm⁻¹ (Figure 6a), reported from both synthetic (Chopelas et al., 1994) and natural ringwoodite (e.g., Tenham meteorite, RRUFF ID R070079). Spectra #4 and #5 show the characteristic major bands at ~713-715 and ~917–920 cm⁻¹ observed in synthetic wadsleyite (Liu et al., 1994). Spectra #1, #2, and #5 each display peaks from two coexisting HP phases, but all of these contain both the major band at ~928 cm⁻¹ and the minor band at ~592 cm⁻¹ assigned to majorite on the basis of both synthetic and natural specimens (Ohtani et al., 2004; Rauch et al., 1996; Zhang et al., 2006). Spectrum #2 contains the major peak at ~797 cm⁻¹ (Figure 6a) assigned to akimotoite, again on the basis of both synthetic (Reynard & Rubie, 1996) and natural (Sixiangkou L6 chondrite; Zhang et al., 2006) specimens. Although the Raman signal of akimotoite in the majorite region is not significant in the spectra. EBSD further confirmed its ilmenite-like structure unambiguously (Figure 7). Spectra #6 and #8 (Figure 6a) yield peaks at ~700, 375, 380, 990, 1035 cm⁻¹, and a comparatively smaller one at ~580 cm⁻¹, similar to other reported instances of albitic jadeite (Baziotis et al., 2023; Baziotis, Ma, et al., 2022). Additionally, spectrum #6 has peaks at 765 and ~630 cm⁻¹ that are characteristic of synthetic hollandite and natural lingunite (Sixiangkou L6 chondrite; Gillet et al., 2000). Spectrum #7 displays a dominant peak at ~977 cm⁻¹ with a shoulder at ~999 cm⁻¹, along with two weak peaks at ~412 and 580 cm⁻¹. All four of these peaks are assigned to tuite on the basis of synthetic γ -Ca₃(PO₄)₂ (Xie, Minitti, et al., 2002) and natural tuite (Suizhou L6 chondrite; Xie et al., 2003). Spectrum #9 shows two peaks, a dominant chromite peak at ~680 cm⁻¹ and a small peak at ~605 cm⁻¹ characteristic of xieite (CaTi₂O₄-type structure; Chen et al., 2008; Chen, Shu, Xie, et al., 2003). The EBSD patterns collected from a chromite clast with crystallographic BSE contrast (Figure 8) are consistent with this result: The BSE-dark areas are indexed with the chromite structure, while the BSE-bright areas within the same clast are indexed as xieite structure.

NWA 12841

The Raman spectra (numbers in parentheses correspond to spectrum number as shown in Figure 6b) of NWA 12841 indicate the presence of ringwoodite (#1, #7), wadsleyite (#1), majorite (#5, #6, #10), akimotoite (#6), albitic-jadeite (#2, #3, #8), lingunite (#3, #8), tuite (#11), and xieite (#13). Furthermore, the EBSD patterns collected from a chromite clast from NWA 12841 (Figure 9) that expresses crystallographic BSE contrast confirm the coexistence of chromite structure (BSE dark) and xieite structure (BSE bright). We also collected EBSD data from an area of NWA 12841 that hosts fine aggregates of akimotoite and majorite (Figures 5b and 7). The EBSD patterns confirm the presence of akimotoite structure.

DISCUSSION

Pressure-Temperature Constraints

Using a variety of in situ analytical techniques, we identified and confirmed the presence of eight high-pressure (HP) phases within the shock melt veins in the L6 ordinary chondrites NWA 4672 and NWA 12841.

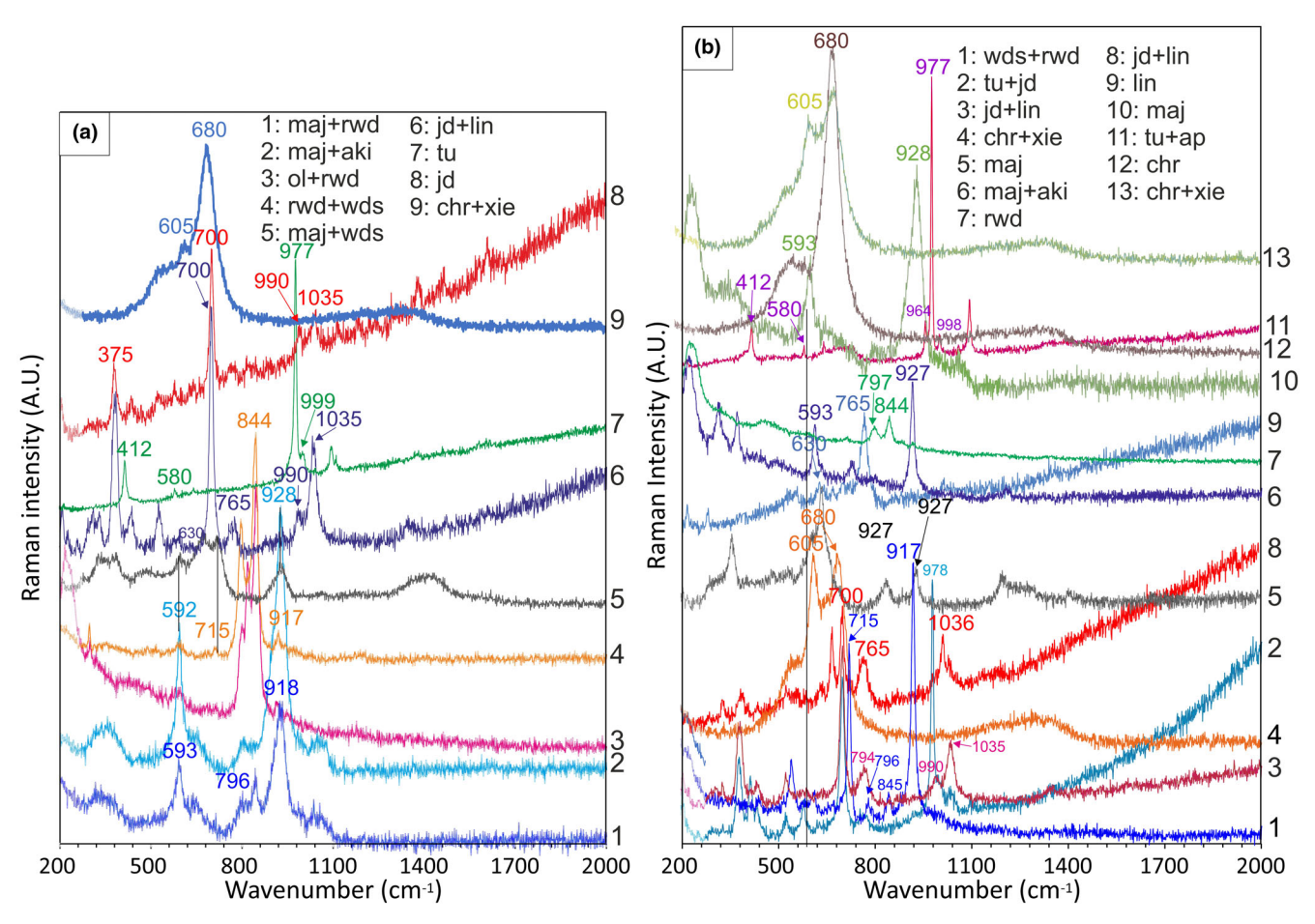


FIGURE 6. Selected Raman spectra of high-pressure minerals identified in (a) NWA 4672 and (b) NWA 12841. Each spectrum corresponds to spot analyses indicated in Figures 4 and 5. Raman peaks characteristic of specific phases are labeled, showing the identification of majorite, ringwoodite, wadsleyite, akimotoite, jadeite, lingunite, tuite, and xieite. The Raman spectra were colocated with microprobe analyses, ensuring that the mineralogical identifications are supported by corresponding chemical compositions. Together, the spectra highlight the diversity of HP assemblages and confirm the mineralogical assignments made from petrographic observations.

The identified HP phases are ringwoodite, majorite, akimotoite, wadsleyite, albitic jadeite, lingunite, tuite, and xieite. These phases can be used as proxies to constrain ranges of pressure–temperature (P–T) conditions that were encountered along the shock and release paths experienced by these two objects.

Although the *absence* of an observation of a phase assemblage is not especially strong evidence, it seems likely that neither meteorite ever reached a peak pressure above 23-25 GPa because of the absence of periclase, coexisting with either bridgmanite or stishovite (Agee et al., 1995). Moreover, peak pressures beyond 25 GPa in chondrites are associated with the formation of distributed intergranular melt, whereas melting in the studied meteorites is limited to veins (Stöffler et al., 2018). The peak pressures would need to have reached the ringwoodite stability range of at 17-23 GPa.

Polycrystalline akimotoite has been synthesized up to a pressure of 23 GPa (Nishi et al., 2022). Similar pressures are also suggested by the observed composition of majoritic garnet, which has been calibrated to (static) pressure by Collerson et al. (2010). While such calibrations provide a useful reference, we note that static experiments are not fully representative of the transient conditions during impact events, and the estimated pressures should be regarded as approximate indicators of peak shock state. Using Collerson's calibration, the electron probe microanalysis (EPMA) of NWA 4672 majoritic garnet gives $P = 22.8 \pm 0.20$ GPa, while for NWA 12841, $P = 23.0 \pm 0.23$ GPa. These estimates are consistent with the P estimates provided by Collerson et al. (2010) for melt veins from four L6 chondrites and with the P range of the liquidus field of majoritic garnet in chondritic melt compositions in static experiments.

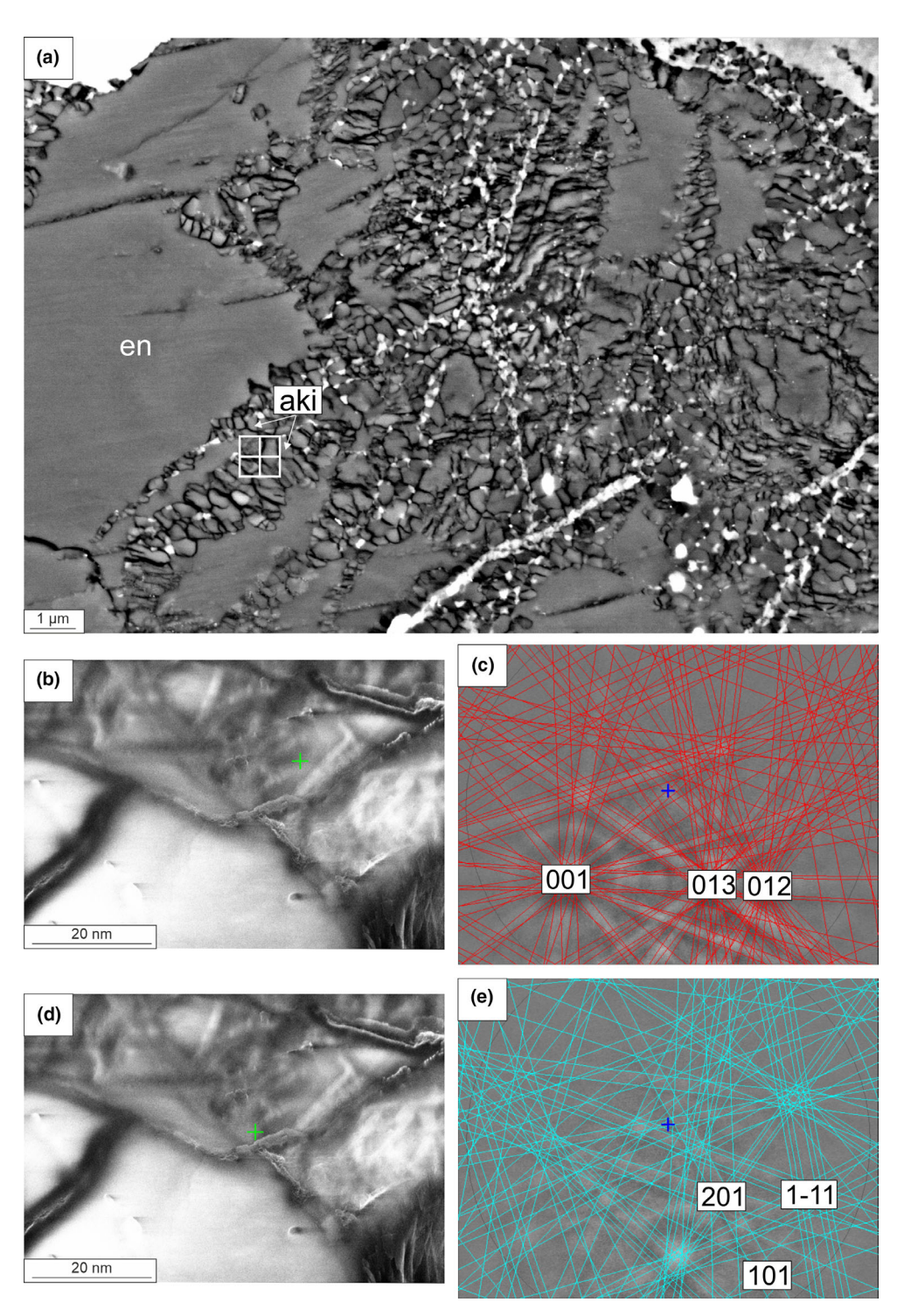


FIGURE 7. (a) High-resolution backscattered electron image of complex fine phase aggregate from akimotoite and majorite region of NWA 12841 shown in Figure 5b. The area marked with a box is further magnified to show locations of individual EBSD acquisitions. The point marked by a green cross in (b) is indexed to the low-pressure phase enstatite in (c), whereas the point marked by a green cross in (d) is indexed to the high-pressure phase akimotoite in (e).

The inference of pressure from jadeite-related phases is currently quite challenging. Although we observed Raman spectra consistent with true jadeite, our

co-located EPMA results show that this material is albitic jadeite, with significant vacancies on M2 and excess Si on M1. Albitic jadeite has not been synthesized yet in any

19455100, 0, Downloaded from https://onlinelibrary.wiley.com/doi/10.1111/maps.70054 by Natl Hellenic Res Fndtn (NHRF), Wiley Online Library on [24/10/2025]. See the Terms

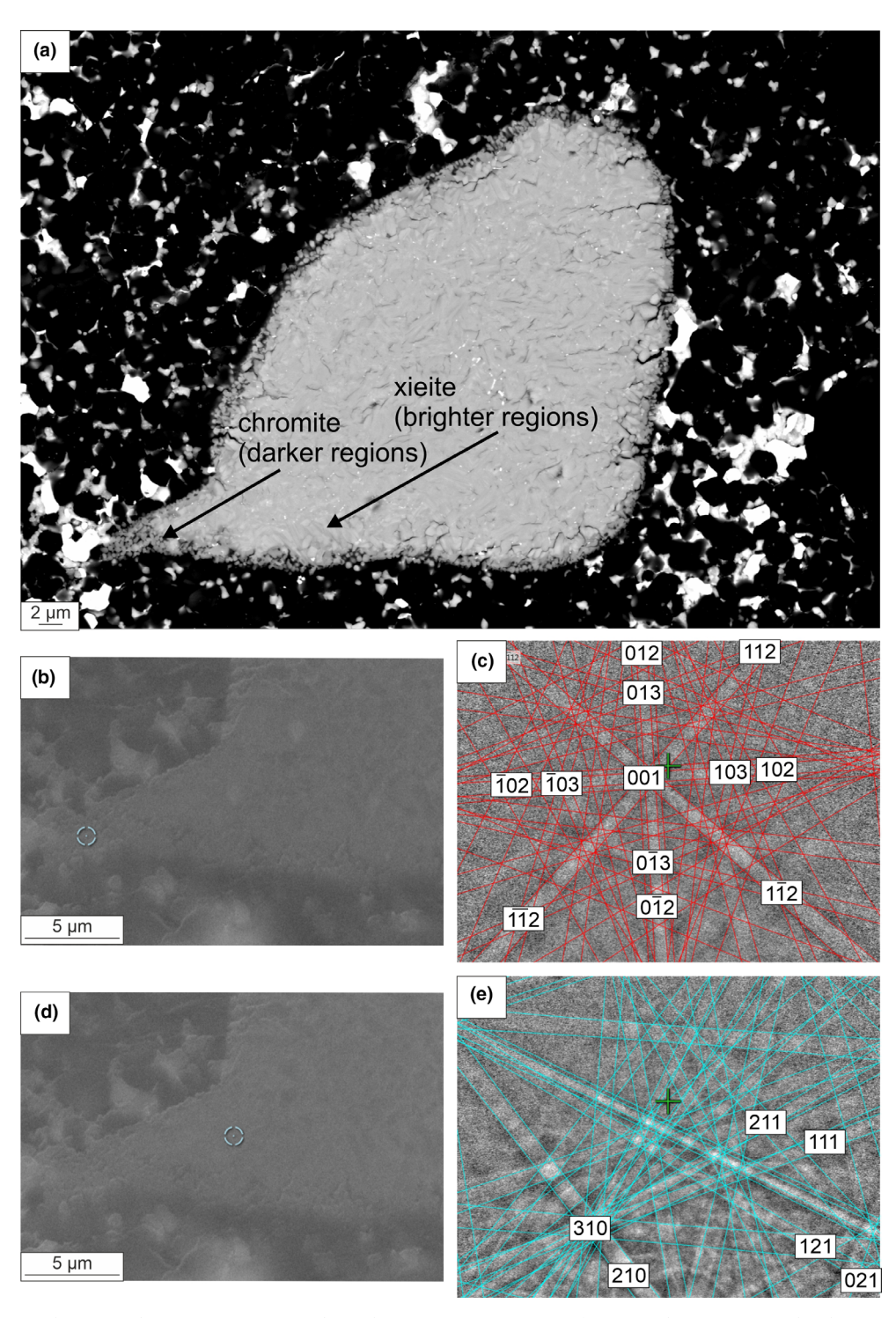


FIGURE 8. (a) Backscattered electron image of a chromite clast in NWA 4672 displaying a shock texture with distinct crystallographic contrast visible despite apparently identical compositions of chromite and xieite. EBSD data acquired at the point marked in (b) indexed to the chromite structure in (c). The pattern acquired at the point marked in (d) is indexed as xieite in (e).

experiment, and therefore, its formation conditions are still poorly understood. In previously documented cases, its coexistence with other HP minerals with known stability ranges has suggested consistent pressure ranges for its formation: coexistence with near endmember majorite implies formation at 18-22 GPa (Baziotis

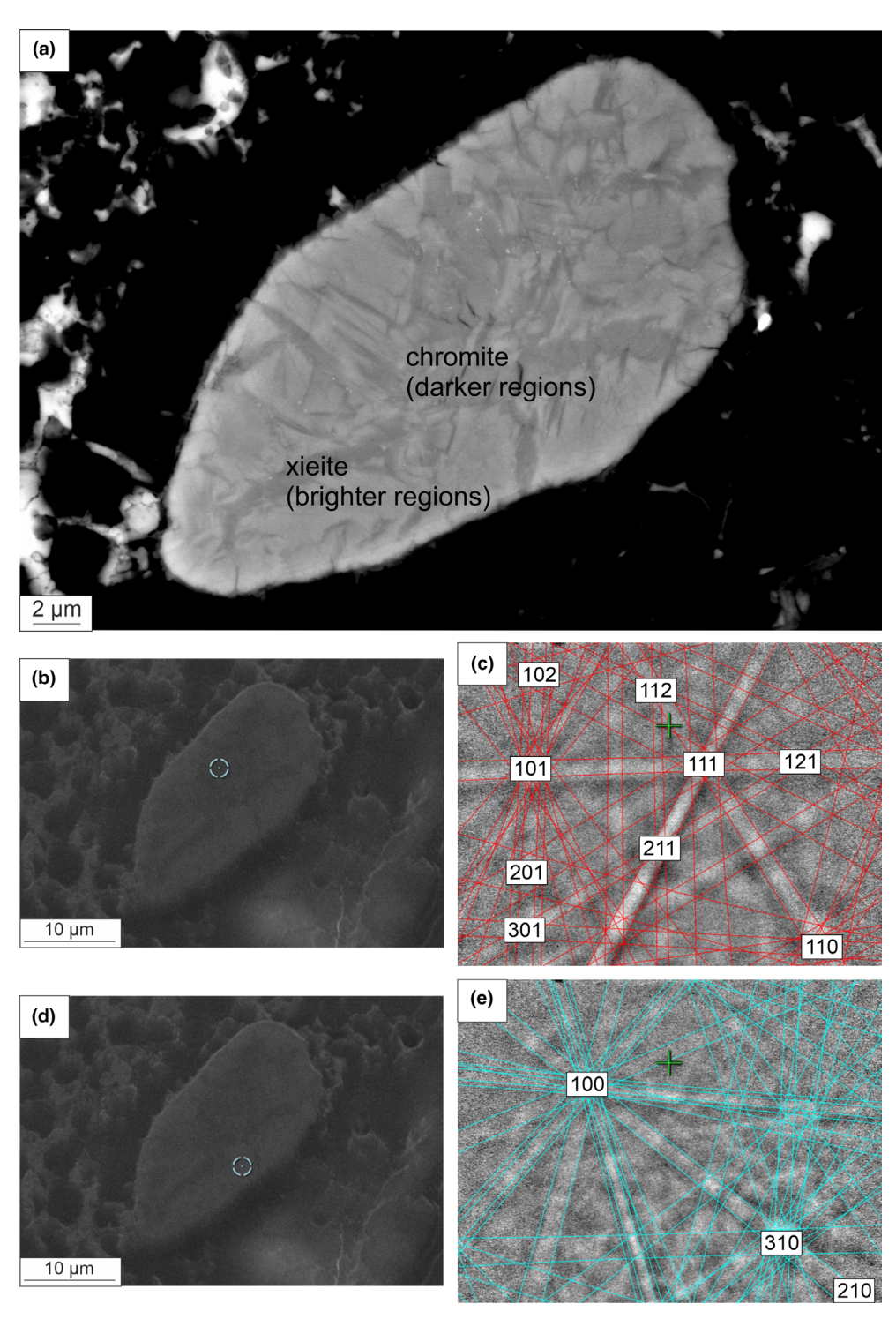


FIGURE 9. (a) Backscattered electron image of a chromite clast in NWA 12841 displaying a shock texture, with crystallographic contrast visible despite apparently identical compositions of chromite and xieite. EBSD data acquired at the point marked in (b) are indexed to the chromite structure in (c). The pattern acquired at the point marked in (d) is indexed as xieite in (e).

et al., 2023; Ma et al., 2022) and with lingunite implies 18–23 GPa (Gasparik, 1989; Liu & El Gorsey, 2007). The most favorable pressure for transformation of feldspar to

homogeneous albitic jadeite rather than stoichiometric jadeite plus a separate silica phase may be as low as ~11.5 GPa (Baziotis et al., 2025).

Tuite likely formed in these meteorites from the transformation of merrillite and chlorapatite, as indicated by the unique texture illustrated in Figure 5e. The minimum conditions for tuite formation vary from $P \sim 12$ GPa at 1100° C (Xie et al., 2016) up to 20–23 GPa at $1900-2000^{\circ}$ C (Murayama et al., 1986; Xie et al., 2003, 2013; Zhai et al., 2014). A similar pressure range is implied by xieite (20–23 GPa at $1800-1950^{\circ}$ C (Chen, Shu, Mao, et al., 2003); >16–18 GPa (Ma et al., 2019)). In contrast, some memory of a lower pressure stage of the shock and release path, at 14-18 GPa, is suggested by the occurrence of wadsleyite (Fei & Bertka, 1999; Katsura et al., 2004; Katsura & Ito, 1989).

The coexistence of minerals demanding peak P of 18–23 GPa and T of 1800–2100°C with those implying lower P (14–18 GPa for wadsleyite and possibly as low as 11.5 GPa for albitic jadeite) indicates small-scale spatial or temporal heterogeneity of the P and T conditions. While extreme spatial gradients in temperature may be created and persist on the time scale of shock and release (and are strongly implied by the presence of discrete melt veins), spatial gradients of pressure over sub-mm distances exceed the elastic limits of minerals (Nagaki et al., 2016). Therefore, the pressure variations recorded are more likely to reflect variations in time (t), with the preservation of minerals developed at various steps along the P-T-t path. This path is controlled by the influence of temperature variations on the kinetics of mineral growth and decomposition (Hu & Sharp, 2022). It is obvious that the melt veins cooled across their liquidus near peak pressure conditions and also that pressure release began before the cooling of the melt veins crossed the solidus or the glass transition, such that pressure decrease occurred in the presence of melt from which phases could grow below the peak pressure. However, cooling must been fast enough to prevent backtransformation to ambient pressure minerals.

High Number of Polymorphs: Indicator of Strong Shock or Observational Bias?

The number of high-pressure polymorphs found in shocked chondrites is often interpreted as a proxy for shock intensity and thermal regime during impact events. Suizhou, an L6 chondrite, stands out in this respect, with a total of 26 distinct HP phases identified within or adjacent to its melt veins (Xie et al., 2025). In contrast, the meteorites studied here—NWA 12841 and NWA 4672—contain a total of eight HP polymorphs each, and many L-type chondrites (including a number of L6) have few or no reported HP phases. This raises a fundamental question: Why have no other meteorites, even those classified with a similar shock stage, matched the polymorph diversity observed in Suizhou?

One explanation would be that Suizhou simply experienced a more extreme shock event than other meteorites. Its mineral assemblage suggests prolonged high-temperature conditions following the initial shock pulse. As Hu and Sharp (2022) emphasize, not only pressure but also the duration of the high-temperature stage and the rate of post-shock cooling are critical for HP phase formation and their preservation. In this view, Suizhou may represent a rare case where a unique combination of physical conditions allowed numerous polymorphs to crystallize and be preserved.

On the other hand, Suizhou has been studied more intensively than most other meteorites, high-resolution techniques such as transmission electron microscopy (TEM), field emission-scanning electron microscopy (SEM), synchrotron X-ray diffraction (XRD), and micro-Raman spectroscopy. These methods are particularly effective at detecting nanocrystalline and minor polymorph phases, many of which would be missed in routine SEM or EPMA work. It is likely that the high polymorph count in Suizhou partly reflects the extent and depth of analysis rather than solely its shock history. As noted by Hu and Sharp (2022), many shocked chondrites may host a greater variety of HP phases than currently recognized, simply because they have not been examined in sufficient detail. Some high-pressure structures, such as poirierite, require detailed local defect characterization at TEM level to be identified. On the other hand, some ferrous high-pressure minerals, such as asimowite and hemleyite, are formed in local iron-rich compositions, deviating from the bulk MV chemistry (Xie et al., 2025). These factors are not controlled by the overall pressure conditions of the meteorites.

Our own findings in NWA 4672 and NWA 12841 support this view. The eight HP polymorphs identified in each meteorite were detected through targeted analysis of shock melt veins using SEM-EDS-EBSD, EPMA, and Raman spectroscopy. It is very possible that additional HP phases exist in these samples, particularly at nanoscales or in less obvious settings, which would require further investigation using TEM or synchrotron-based methods. In that sense, the number of HP phases in any given meteorite is not only a product of its shock history but also of how thoroughly and at what scales it has been studied.

Compositional factors may also play a role. Differences in mineral modes or local chemistry can affect which HP phases are likely to form. For instance, ringwoodite formation is favored in olivine-rich domains, whereas phases like majorite or lingunite depend on the presence of pyroxene or feldspathic material. Even subtle differences in Fe/Mg ratio or volatile content can shift stability fields. Therefore, some of the variations in polymorph diversity among shocked L chondrites may

also reflect lithological/mineral chemical differences rather than just shock conditions.

In summary, while the high number of HP polymorphs in Suizhou likely reflects both specific P-Tconditions and specific analytical coverage, we suggest that many meteorites—especially those with welldeveloped melt vein systems—may harbor more polymorphs than currently reported. It is best to avoid drawing strong conclusions about shock conditions in meteorites from the absence of detected phases until they have been searched for in adequate detail. The relatively high HP phase counts in both NWA 4672 and NWA 12841 support this possibility. However, recovery and annealing processes may also play a significant role in the absence of HP phases, particularly beyond certain P-T conditions (Hu & Sharp, 2022). Broader and deeper investigations of other L6 chondrites using highresolution techniques could reveal that HP phase diversity is much more common than previously thought.

Fragmentation Behavior and Shock-Related Textures in L6 Ordinary Chondrites

So far, we have focused our discussion of the shock features in NWA 4672 and NWA 12841 on their implications for collisional processing on their parent body (or bodies). However, another key step in the natural history of any meteorite is its entry into and passage through the Earth's atmosphere on its way to the ground. In this regard, it is thought that shock-related textures may have a strong influence on fragmentation behavior during atmospheric entry (Popova et al., 2013). Hence, we discuss here the relevance of dense networks of MVs, metal-sulfide segregations, dark shock zones, and brecciation for fragmentation, with implications for the size distribution of recovered fragments of L6 chondrites.

The mechanical response of meteoroids during atmospheric entry depends not only on external parameters such as entry velocity, angle, and size but also on intrinsic material properties-specifically porosity, cohesion, and the spatial distribution of shock-related heterogeneities. In particular, Brykina and Egorova (2021) demonstrated that the shock melt veins in L6 chondrites often form interconnected systems enriched in metal and sulfides, which can create zones of mechanical weakness and increase the susceptibility to fragmentation. Popova et al. (2013) also suggested that metal-rich melt veins may locally weaken the meteorite through differential thermal expansion—despite the typical increase in disseminated material strength associated with shock consolidation. In NWA 12841, for instance, MVs with variable width intersect throughout the sample, often associated with finegrained recrystallized zones and micro-breccias, suggesting intense shock damage. NWA 4672 similarly displays vein networks that likely reflect an extensive impact history. Interestingly, this type of effect is not exclusive to L chondrites. LL chondrite NWA 757 shows adjacent MVs of distinct high-pressure assemblages and microstructures, indicating a second shock—shear event occurred during the partial quenching of the initial MV, likely caused by complex propagation of shock wave on the parent body (Hu & Sharp, 2016).

Although petrological observations alone cannot reconstruct the exact dynamics of atmospheric breakup, they can provide strong clues about pre-existing structural weaknesses that may have predisposed the meteoroid to fragmentation. Features such as penetrative MV networks, abrupt vein terminations, and textural asymmetries (e.g., dark shock zones) may act as failure foci under aerodynamic loading. The presence of such features suggests that L6 chondrites like NWA 4672 and NWA 12841 would likely follow a highly fragmentary breakup pattern upon atmospheric entry—consistent with models for structurally heterogeneous meteoroids.

This interpretation finds further support from observed falls such as the Viñales meteorite. Upon atmospheric entry. Viñales broke up into numerous pieces, with hundreds of individual fragments recovered -ranging in mass from a few grams up to several kilograms (Meteoritical Bulletin; Yin & Dai, 2021; main mass is 10.6 kg). Petrological examination of Viñales reveals a dense network of variable thickness melt veins, many of which contain segregated metal-rich layers, visible at both microscopic and macroscopic scales (see e.g., figure 1 in Baziotis et al., 2023). Moreover, Brykina and Egorova (2021) examined the mass distribution of fragments resulting from atmospheric disruptions (e.g., Chelyabinsk meteorite) and showed that meteoroids with internal heterogeneity (especially those with dense MV networks) are more likely to fragment into a larger number of smaller pieces. Their results highlight how internal petrophysical complexity—formed by parent body impacts and later modified by secondary collisions —can directly influence fragmentation outcomes. The textures seen in NWA 4672 and NWA 12841 are similar to those in Viñales, suggesting efficient fragmentation of these meteoroids as well.

In summary, while the studied samples do not preserve direct evidence of atmospheric breakup, their internal structure—characterized by extensive shock-related heterogeneities—supports the idea that material properties shaped by impact histories play a critical role in controlling fragmentation behavior during the Earth's atmospheric entry (e.g., Baziotis, Ma, et al., 2022; Baziotis, Xydous, et al., 2022; Brykina & Egorova, 2021; Popova et al., 2013; Yin & Dai, 2021). Hence, the discovery of paired stones for these two finds seems quite probable.

19455100, 0, Downloaded from https://onlinelibrary.wilej.com/doi/10.1111/maps.70054 by Natl Hellenic Res Firdtn (NHRP), Wiley Online Library on [24/10/2025]. See the Terms and Conditions (https://onlinelibrary.wiley.com/terms-and-conditions) on Wiley Online Library on [24/10/2025]. See the Terms and Conditions (https://onlinelibrary.wiley.com/doi/10.1111/maps.70054 by Natl Hellenic Res Firdtn (NHRP), Wiley Online Library on [24/10/2025]. See the Terms and Conditions (https://onlinelibrary.wiley.com/doi/10.1111/maps.70054 by Natl Hellenic Res Firdtn (NHRP), Wiley Online Library on [24/10/2025]. See the Terms and Conditions (https://onlinelibrary.wiley.com/doi/10.1111/maps.70054 by Natl Hellenic Res Firdtn (NHRP), Wiley Online Library on [24/10/2025]. See the Terms and Conditions (https://onlinelibrary.wiley.com/doi/10.1111/maps.70054 by Natl Hellenic Res Firdtn (NHRP), Wiley Online Library on [24/10/2025]. See the Terms and Conditions (https://onlinelibrary.wiley.com/doi/10.1111/maps.70054 by Natl Hellenic Res Firdtn (NHRP), Wiley Online Library on [24/10/2025]. See the Terms and Conditions (https://onlinelibrary.wiley.com/doi/10.1111/maps.70054 by Natl Hellenic Res Firdtn (NHRP), Wiley Online Library on [24/10/2025]. See the Terms and Conditions (https://onlinelibrary.wiley.com/doi/10.1111/maps.70054 by Natl Hellenic Res Firdtn (NHRP), Wiley Online Library on [24/10/2025]. See the Terms and Conditions (https://onlinelibrary.wiley.com/doi/10.1111/maps.70054 by Natl Hellenic Res Firdtn (NHRP), Wiley Online Library on [24/10/2025]. See the Terms and Conditions (https://onlinelibrary.wiley.com/doi/10.1111/maps.70054 by Natl Hellenic Res Firdtn (NHRP), Wiley Online Library on [24/10/2025]. See the Terms and Conditions (https://onlinelibrary.wiley.com/doi/10.1111/maps.70054 by Natl Hellenic Res Firdtn (NHRP), Wiley Online Library on [24/10/2025]. See the Terms and Conditions (https://onlinelibrary.wiley.com/doi/10.1111/maps.70054 by Natl Hellenic Res Firdtn (NHRP), Wiley Online Library on [24/10/2025]. See the Terms

CONCLUSIONS

NWA 4672 and NWA 12841 each host eight highpressure (HP) mineral species. Both meteorites host HP minerals defining peak shock conditions of 18-23 GPa and 1800-2100°C as well as minerals preserving lower pressure conditions that most likely grew during partial release from the peak shock state. The HP minerals and the sizes of their host melt veins (MVs) yield constraints on the pressure-temperature-time paths experienced by both meteorites as a strong shock and following release wave passed through them. Although both meteorites contain multiple melt veins with a range of thicknesses, petrographic examination has not yet shown any instances where one melt vein offsets, truncates, or overprints another and thereby indicates that they are of different generations (Chen & Xie, 2007). Thus, it remains unclear whether more than one impact is recorded. Nonetheless, the density of melt veins is sufficient to suggest that the recovered specimens are likely fragments of larger objects that broke up on atmospheric entry. Although NWA 4672 and NWA 12841 host more HP phases than recognized in most L6 chondrites, they are still far less than in the intensively studied Suizhou meteorite. These results contribute to the of the L-chondrites. shock record Additional petrographic work and high-resolution study will be required to test whether the differences in HP phase detection among L6 specimens are an observational bias or a true difference in the outcome of their shock histories.

Acknowledgments—Dan Topa and Wencke Wegner are acknowledged for assistance in the acquisition of EPMA data at the NHMW. I.B. received support from the SYNTHESYS Project, which is financed by the European Community Research Infrastructure Action under the FP7 "Capacities" Program. I.B. also thanks the Wolfgang Pauli Institute (WPI) Vienna, which provided funds for travel and accommodation. We thank the associate editor Wolf Reimold for editorial handling and two anonymous reviewers for their constructive comments, which improved the original manuscript.

Conflict of Interest Statement—None of the authors have a conflict of interest to disclose.

Data Availability Statement—The data that support the findings of this study are available from the corresponding author upon reasonable request.

Editorial Handling-Dr. Wolf Reimold

REFERENCES

- Agee, C. B., Li, J., Shannon, M. C., and Circone, S. 1995. Pressure-Temperature Phase Diagram for the Allende Meteorite. *Journal of Geophysical Research: Solid Earth* 100(B9): 17725–40.
- Akaogi, M. 2022. High-Pressure Minerals from the Earth's Mantle and in Shocked Meteorites. In *High-Pressure Silicates and Oxides*, 187–200. Singapore: Springer.
- Baziotis, I., Ma, C., Klemme, S., Berndt, J., Tschauner, O., and Asimow, P. D. 2025. The High-Pressure, Vacancy-Stabilized Component in Clinopyroxenes. *American Mineralogist* 110: 1472–80. https://doi.org/10.2138/am-2024-9609.
- Baziotis, I., Xydous, S., Papoutsa, A., Hu, J., Ma, C., Klemme, S., and Asimow, P. D. 2022. Jadeite and Related Species in Shocked Meteorites: Limitations on Inference of Shock Conditions 107: 1868–77.
- Baziotis, I. P., Ma, C., Guan, Y., Ferrière, L., Xydous, S., Hu, J., Kipp, M. A., Tissot, F. L., and Asimow, P. D. 2022. Unique Evidence of Fluid Alteration in the Kakowa (L6) Ordinary Chondrite. *Scientific Reports* 12: 1–15.
- Baziotis, I. P., Xydous, S., Papoutsa, A., Hu, J., Ma, C., Ferrière, L., Klemme, S., Berndt, J., and Asimow, P. D. 2023. Investigation of the Shocked Viñales Ordinary Chondrite (L6) Meteorite Fall–Implications for Shock Classification, Fragmentation, and Collision Dynamics. *Icarus* 390: 115326.
- Bindi, L., Brenker, F. E., Nestola, F., Koch, T. E., Prior, D.
 J., Lilly, K., Krot, A. N., Bizzarro, M., and Xie, X. 2019.
 Discovery of Asimowite, the Fe-Analog of Wadsleyite, in Shock-Melted Silicate Droplets of the Suizhou L6 and the Quebrada Chimborazo 001 CB3. 0 Chondrites. *American Mineralogist* 104: 775–78.
- Bindi, L., Chen, M., and Xie, X. 2017. Discovery of the Fe-Analogue of Akimotoite in the Shocked Suizhou L6 Chondrite. *Scientific Reports* 7: 1–8.
- Bindi, L., Shim, S. H., Sharp, T. G., and Xie, X. 2020. Evidence for the Charge Disproportionation of Iron in Extraterrestrial Bridgmanite. *Science Advances* 6: eaay7893. https://doi.org/10.1126/sciadv.aay7893.
- Binns, R. A., Davis, R. J., and Reed, S. J. B. 1969. Ringwoodite, Natural (Mg, Fe)₂SiO₄ Spinel in the Tenham Meteorite. *Nature* 221: 943–44.
- Brykina, I. G., and Egorova, L. A. 2021. On the Mass Distribution of Fragments of an Asteroid Disrupted in the Earth's Atmosphere. *Advances in Astronomy* 2021: 9914717.
- Chen, M., and El Goresy, A. 2000. The Nature of Maskelynite in Shocked Meteorites: Not Diaplectic Glass but a Glass Quenched from Shock-Induced Dense Melt at High Pressures. *Earth and Planetary Science Letters* 179: 489–502.
- Chen, M., Shu, J., and Mao, H. K. 2008. Xieite, a New Mineral of High-Pressure FeCr₂O₄ Polymorph. *Chinese Science Bulletin* 53: 3341–45.
- Chen, M., Shu, J., Mao, H. K., Xie, X., and Hemley, R. J. 2003. Natural Occurrence and Synthesis of Two New Postspinel Polymorphs of Chromite. *Proceedings of the National Academy of Sciences of the United States of America* 100: 14651–54.
- Chen, M., Shu, J., Xie, X., and Mao, H. K. 2003. Natural CaTi₂O₄-Structured FeCr₂O₄ Polymorph in the Suizhou Meteorite and its Significance in Mantle Mineralogy. *Geochimica et Cosmochimica Acta* 67: 3937–42.

Chen, M., and Xie, X. 2007. Two Distinct Assemblages of High-Pressure Liquidus Phases in Shock Veins of the Sixiangkou Meteorite. *Meteoritics and Planetary Science* 43: 823–28.

- Chopelas, A., Boehler, R., and Ko, T. 1994. Thermodynamics and Behavior of γ-Mg₂SiO₄ at High Pressure: Implications for Mg₂SiO₄ Phase Equilibrium. *Physics and Chemistry of Minerals* 21: 351–59.
- Collerson, K. D., Williams, Q., Kamber, B. S., Omori, S., Arai, H., and Ohtani, E. 2010. Majoritic Garnet: A New Approach to Pressure Estimation of Shock Events in Meteorites and the Encapsulation of Sub-Lithospheric Inclusions in Diamond. *Geochimica et Cosmochimica Acta* 74: 5939–57.
- Fei, Y., and Bertka, C. M. 1999. Phase Transitions in the Earth's Mantle and Mantle Mineralogy. *Mantle Petrology:* Field Observations and High Pressure Experimentation 6: 189–207.
- Gasparik, T. 1989. Transformation of Enstatite—Diopside— Jadeite Pyroxenes to Garnet. Contributions to Mineralogy and Petrology 102: 389–405.
- Ghosh, S., Tiwari, K., Miyahara, M., Rohrbach, A., Vollmer, C., Stagno, V., Ohtani, E., and Ray, D. 2021. Natural Fe-Bearing Aluminous Bridgmanite in the Katol L6 Chondrite. Proceedings of the National Academy of Sciences of the United States of America 118: e2108736118.
- Gillet, P., Chen, M., Dubrovinsky, L., and Goresy, A. E. 2000. Natural NaAlSi₃O₈-Hollandite in the Shocked Sixiangkou Meteorite. *Science* 287: 1633–36.
- Hu, J., and Sharp, T. G. 2016. High-Pressure Phases in Shock-Induced Melt of the Unique Highly Shocked LL 6 Chondrite Northwest Africa 757. Meteoritics & Planetary Science 51: 1353–69.
- Hu, J., and Sharp, T. G. 2022. Formation, Preservation and Extinction of High-Pressure Minerals in Meteorites: Temperature Effects in Shock Metamorphism and Shock Classification. *Progress in Earth and Planetary Science* 9: 1–22
- Katsura, T., and Ito, E. 1989. The System Mg₂SiO₄-Fe₂SiO₄ at High Pressures and Temperatures: Precise Determination of Stabilities of Olivine, Modified Spinel, and Spinel. *Journal of Geophysical Research: Solid Earth* 94(B11): 15663–70.
- Katsura, T., Yamada, H., Nishikawa, O., Song, M., Kubo, A., Shinmei, T., Yokoshi, S., et al. 2004. Olivine-Wadsleyite Transition in the System (Mg, Fe)₂SiO₄. Journal of Geophysical Research: Solid Earth 109(B2): 1–12.
- Korochantseva, E. V., Trieloff, M., Lorenz, C. A., Buykin, A. I., Ivanova, M. A., Schwarz, W. H., and Jessberger, E. K. 2007. L-Chondrite Asteroid Breakup Tied to Ordovician Meteorite Shower by Multiple Isochron 40Ar-39Ar Dating. Meteoritics & Planetary Science 42: 113–130.
- Liu, L. G., and El Gorsey, A. 2007. High-Pressure Phase Transitions of the Feldspars, and Further Characterization of Lingunite. *International Geology Review* 49: 854–860.
- Liu, L. G., Mernagh, T. P., and Irifune, T. 1994. High Pressure Raman Spectra of β-Mg₂SiO₄, γ-Mg₂SiO₄, MgSiO₃-Ilmenite and MgSiO₃-Perovskite. Journal of Physics and Chemistry of Solids 55: 185–193.
- Ma, C. 2018. A Closer Look at Shocked Meteorites: Discovery of New High-Pressure Minerals. American Mineralogist 103: 1521–22.
- Ma, C., Tschauner, O., Beckett, J. R., Liu, Y., Greenberg, E., and Prakapenka, V. B. 2019. Chenmingite, FeCr₂O₄ in the

- CaFe₂O₄-Type Structure, a Shock-Induced, High-Pressure Mineral in the Tissint Martian Meteorite 104: 1521–25.
- Ma, C., Tschauner, O., Beckett, J. R., Liu, Y., Rossman, G. R., Sinogeikin, S. V., and Taylor, L. A. 2016. Ahrensite, γ-Fe₂SiO₄, a New Shock-Metamorphic Mineral from the Tissint Meteorite: Implications for the Tissint Shock Event on Mars. *Geochimica et Cosmochimica Acta* 184: 240–256.
- Ma, C., Tschauner, O., Kong, M., Beckett, J. R., Greenberg, E., Prakapenka, V. B., and Lee, Y. 2022. A High-Pressure, Clinopyroxene-Structured Polymorph of Albite in Highly Shocked Terrestrial and Meteoritic Rocks. *American Mineralogist* 107: 625–630.
- Mason, B., Nelen, J., and White, J. S., Jr. 1968. Olivine-Garnet Transformation in a Meteorite. *Science* 160: 66–67.
- Miyahara, M., Ohtani, E., and Yamaguchi, A. 2017. Albite Dissociation Reaction in the Northwest Africa 8275 Shocked LL Chondrite and Implications for its Impact History. *Geochimica et Cosmochimica Acta* 217: 320–333
- Murayama, J. K., Nakai, S., Kato, M., and Kumazawa, M. 1986. A Dense Polymorph of Ca₃(PO₄)₂: A High Pressure Phase of Apatite Decomposition and its Geochemical Significance. *Physics of the Earth and Planetary Interiors* 44: 293–303.
- Nagaki, K., Kadono, T., Sakaiya, T., Kondo, T., Kurosawa, K., Hironaka, Y., Shigemori, K., and Arakawa, M. 2016. Recovery of Entire Shocked Samples in a Range of Pressure from~ 100 GP a to Hugoniot Elastic Limit. *Meteoritics & Planetary Science* 51: 1153–62.
- Nishi, M., Kaneko, A., Ohgidani, H., Dekura, H., Kakizawa, S., Kawaguchi, S., and Kondo, T. 2022. Bridgmanite Freezing in Shocked Meteorites Due to Amorphization-Induced Stress. Geophysical Research Letters 49: e2022GL098231.
- Ohtani, E., Kimura, Y., Kimura, M., Takata, T., Kondo, T., and Kubo, T. 2004. Formation of High-Pressure Minerals in Shocked L6 Chondrite Yamato 791384: Constraints on Shock Conditions and Parent Body Size. *Earth and Planetary Science Letters* 227: 505–515.
- Popova, O. P., Jenniskens, P., Emel'yanenko, V., Kartashova,
 A., Biryukov, E., and Khaibrakhmanov, S. 2013.
 Chelyabinsk Airburst, Damage Assessment, Meteorite
 Recovery, and Characterization. Science 342: 1069–73.
- Price, G. D., Putnis, A., Agrell, S. O., and Smith, D. G. W. 1983. Wadsleyite, Natural Beta-(Mg, Fe)₂SiO₄ from the Peace River Meteorite. *The Canadian Mineralogist* 21: 29–35
- Putnis, A., and Price, G. D. 1979. High-Pressure (Mg, Fe)₂SiO₄ Phases in the Tenham Chondritic Meteorite. *Nature* 280: 217–18.
- Rauch, M., Keppler, H., Häfner, W., Poe, B., and Wokaun, A. 1996. A Pressure-Induced Phase Transition in MgSiO₃-Rich Garnet Revealed by Raman Spectroscopy. *American Mineralogist: Journal of Earth and Planetary Materials* 81: 1289–92.
- Reynard, B., and Rubie, D. C. 1996. High-Pressure, High-Temperature Raman Spectroscopic Study of Ilmenite-Type MgSiO₃. American Mineralogist 81: 1092–96.
- Saikia, B. J., Parthasarathy, G., and Borah, R. R. 2022. High-Pressure Polymorphs of Olivine and Silica in Kamargaon (L6) Chondrite by Laser Micro-Raman and XRD Studies. *Journal of Earth System Science* 131: 38.
- Sazonova, L. V., Fel'dman, V. I., Kozlov, E. A., Dubrovinskaya, N. A., and Dubrovinskii, L. S. 2006.

- Genesis of Ringwoodite during Metamorphism Induced by Impact Waves: Experimental Data. *Geochemistry International* 44: 137–142.
- Schmitz, B., Yin, Q. Z., Sanborn, M. E., Tassinari, M., Caplan, C. E., and Huss, G. R. 2016. A New Type of Solar-System Material Recovered from Ordovician Marine Limestone. *Nature Communications* 7: ncomms11851.
- Sharp, T. G., Lingemann, C. M., Dupas, C., and Stoffler, D. 1997. Natural Occurrence of MgSiO₃-Ilmenite and Evidence for MgSiO₃-Perovskite in a Shocked L Chondrite. *Science* 277: 352–55.
- Simopoulou, M., Baziotis, I., Ferrière, L., Hu, J., Sanchez-Valle, C., Gamaletsos, P. N., Palles, D., et al. 2025. Raman Study of the Slobodka Ordinary Chondrite. *Journal of Raman Spectroscopy*. https://doi.org/10.1002/jrs.6833.
- Smith, J. V., and Mason, B. 1970. Pyroxene-Garnet Transformation in Coorara Meteorite. *Science* 168: 832–33.
- Stishov, S. M. 1961. A New Dense Modification of Silica. *Geokhimiya* 10: 837–39.
- Stöffler, D., Hamann, C., and Metzler, K. 2018. Shock Metamorphism of Planetary Silicate Rocks and Sediments: Proposal for an Updated Classification System. *Meteoritics & Planetary Science* 53: 5–49.
- Tomioka, N., and Fujino, K. 1997. Natural (Mg, Fe)SiO₃-Ilmenite and-Perovskite in the Tenham Meteorite. *Science* 277: 1084–86.
- Tomioka, N., and Fujino, K. 1999. Akimotoite, (Mg, Fe)SiO₃, a New Silicate Mineral of the Ilmenite Group in the Tenham Chondrite. *American Mineralogist* 84: 267–271.
- Tomioka, N., Mori, H., and Fujino, K. 2000. Shock-Induced Transition of NaAlSi₃O₈ Feldspar into a Hollandite Structure in a L6 Chondrite. *Geophysical Research Letters* 27: 3997–4000.
- Tomioka, N., and Okuchi, T. 2017. A New High-Pressure Form of Mg₂SiO₄ Highlighting Diffusionless Phase Transitions of Olivine. *Scientific Reports* 7: 1–9.
- Tomioka, N., Okuchi, T., Iitaka, T., Miyahara, M., Bindi, L., and Xie, X. 2020. Poirierite, IMA 2018-026b, in: CNMNC Newsletter 54. European Journal of Mineralogy 32. https://doi.org/10.5194/ejm-32-275-2020.
- Tschauner, O., Asimow, P. D., Kostandova, N., Ahrens, T. J., Ma, C., Sinogeikin, S., Liu, Z., Fakra, S., and Tamura, N. 2009. Ultrafast Growth of Wadsleyite in Shock-Produced Melts and its Implications for Early Solar System Impact

SUPPORTING INFORMATION

Additional supporting information may be found in the online version of this article.

- Processes. Proceedings of the National Academy of Sciences of the United States of America 106: 13691–95.
- Tschauner, O., Ma, C., Beckett, J. R., Prescher, C., Prakapenka, V. B., and Rossman, G. R. 2014. Discovery of Bridgmanite, the most Abundant Mineral in Earth, in a Shocked Meteorite. *Science* 346: 1100–1102.
- Xie, X., Bindi, L., Chen, M., and Gu, X. 2025. The Suizhou Meteorite: A Treasure Trove of High-Pressure Minerals. *Acta Geochimica*: 1–15. https://doi.org/10.1007/s11631-025-00774-x.
- Xie, X., Gu, X., and Chen, M. 2016. An Occurrence of Tuite, γ-Ca₃(PO₄)₂, Partly Transformed from Ca-Phosphates in the Suizhou Meteorite. *Meteoritics & Planetary Science* 51: 195–202.
- Xie, X., Gu, X., Yang, H., Chen, M., and Li, K. 2020. Wangdaodeite, the LiNbO₃-Structured High-Pressure Polymorph of Ilmenite, a New Mineral from the Suizhou L6 Chondrite. *Meteoritics & Planetary Science* 55: 184–192
- Xie, X., Minitti, M. E., Chen, M., Mao, H. K., Wang, D., Shu, J., and Fei, Y. 2002. Natural High-Pressure Polymorph of Merrillite in the Shock Veins of the Suizhou Meteorite. Geochimica et Cosmochimica Acta 66: 2439–44.
- Xie, X., Minitti, M. E., Chen, M., Mao, H. K., Wang, D., Shu, J., and Fei, Y. 2003. Tuite, γ-Ca₃(PO₄)₂: A New Mineral from the Suizhou L6 Chondrite. *European Journal of Mineralogy* 15: 1001–5.
- Xie, X., Zhai, S., Chen, M., and Yang, H. 2013. Tuite, γ-Ca₃(PO₄)₂, Formed by Chlorapatite Decomposition in a Shock Vein of the Suizhou L6 Chondrite. *Meteoritics & Planetary Science* 48: 1515–23.
- Xie, Z., Tomioka, N., and Sharp, T. G. 2002. Natural Occurrence of Fe₂SiO₄-Spinel in the Shocked Umbarger L6 Chondrite. *American Mineralogist* 87: 1257–60.
- Yin, F., and Dai, D. 2021. Petrology and Mineralogy of the Viñales Meteorite, the Latest Fall in Cuba. *Science Progress* 104: 00368504211019859.
- Zhai, S., Akaogi, M., Kojitani, H., Xue, W., and Ito, E. 2014. Thermodynamic Investigation on β-and γ-Ca₃(PO₄)₂ and the Phase Equilibria. *Physics of the Earth and Planetary Interiors* 228: 144–49.
- Zhang, A., Hsu, W., Wang, R., and Ding, M. 2006. Pyroxene Polymorphs in Melt Veins of the Heavily Shocked Sixiangkou L6 Chondrite. *European Journal of Mineralogy* 18: 719–726.

Figure S1. Microphotograph of a cut surface of the hand specimen of NWA 4672 (NHMW-N4148). It shows a pale brown groundmass, a complex network of MVs, and a thin fusion crust (upper right).